Rate-Integrating Gyroscope Operation in The Non-Linear Regime

D. Vatanparvar and A. M. Shkel

MicroSystems Laboratory, University of California, Irvine
Irvine, California
USA

Inertial Sensors and Systems 2022
Braunschweig, Germany

978-1-6654-9021-4/22/$31.00 ©2022 IEEE

Abstract

In Coriolis vibratory Rate-Integrating Gyroscopes (RIG), a higher electrical Signal-to-Noise Ratio (SNR) provides an improved resolution for measuring the orientation of the oscillation pattern. Therefore, precession due to a smaller angular rotation can be detected by maximizing the vibration amplitude. On the other hand, the contribution of non-linear mechanisms to the resonator dynamics, the measurements, and the control grows in complexity with the oscillation amplitude. This paper studies the trade-offs between achieving a higher SNR through increasing the oscillation amplitude and the adverse effects of non-linear mechanisms in RIG.

As part of our study, we derived analytical equations to demonstrate that by operating a RIG in the non-linear regime, electrostatically-induced amplitude-frequency coupling results in an angle-dependent anisoelasticity. Anisoelasticity was shown to reduce angular gain and introduce angle-dependent biases in measurements despite utilizing a quadrature control for suppressing ellipticity. We proposed a modified Whole Angle (WA) control, which utilizes a non-linear feedback loop to compensate for the amplitude-frequency coupling along the X and Y axes. By implementing the control with a Micro-Electro-Mechanical System (MEMS) Dual Foucault Pendulum (DFP) gyroscope, we were able to operate the RIG with a vibration amplitude equal to 15% of the capacitive gap size and reduce ellipticity by 100 times. The magnitude of control voltages for compensation of nonlinearity was shown to depend on the biasing voltages, which were intentionally applied for mode-matching.

Based on our observations, we conjectured that impractically large control voltages coupled with phase drifts in electronics degrade the stability of RIG when operated in the non-linear regime. Our results highlight the limitations of feedback compensation methods in RIG and the need for fabrication of structurally symmetric micro-gyroscopes for high-resolution and high-accuracy angle measurements.

1. Introduction

An ideal Coriolis Vibratory Gyroscope (CVG) for direct angle measurements comprises a 2-Degrees of Freedom (2-DoF) mechanical resonator with identical resonant frequencies and negligible energy dissipation. In this ideal resonator, the two resonant modes are coupled only through the Coriolis forces.

The equation of motion (EOM) of an ideal RIG in a non-inertial frame, “attached” to the sensing element, is shown below:

$$\begin{bmatrix}\ddot{x}\\ \ddot{y}\end{bmatrix} + 2\kappa\Omega\begin{bmatrix}0 & -1\\ 1 & 0\end{bmatrix}\begin{bmatrix}\dot{x}\\ \dot{y}\end{bmatrix} + \begin{bmatrix}\omega_n^2 & 0\\ 0 & \omega_n^2\end{bmatrix}\begin{bmatrix}x\\ y\end{bmatrix} = 0, \quad (1)$$

where x and y represent the displacement of the resonator along the reference coordinates X and Y; the parameters Ω, κ, and ω_n denote the angular velocity of rotation, the angular gain of the CVG, and the angular velocity of oscillation, respectively. The solution to this homogeneous differential equation with an initial condition of ($x(0) = a$, $\dot{x}(0) = \dot{y}(0) = y(0) = 0$) is

$$\begin{cases} x = a\,cos\,(\theta)\,cos\,(\omega_n t) \\ y = a\,sin\,(\theta)\,cos\,(\omega_n t) \end{cases}, \quad \theta = -\kappa \int \Omega dt \quad (2)$$

By resorting to the mass-spring representation of the CVG, it is noted that the expression in Eq. (2) represents a mass oscillating along a straight line orientated at the angle θ that is equal to the time-integration of the input angular rate (Ω). The evolution of the oscillation pattern is shown in Fig. 1(a), (c) for a more general elliptical oscillation. The energy transfer between the vibration along the X and Y axes is referred to as precession. It should be noted that precession is only observed in the non-inertial frame, as shown in Fig. 1(b), (c).

In the ideal case, the pattern angle (θ) can be estimated based on the amplitude of vibration along the X and Y axes and utilized for sensing the input rotation.

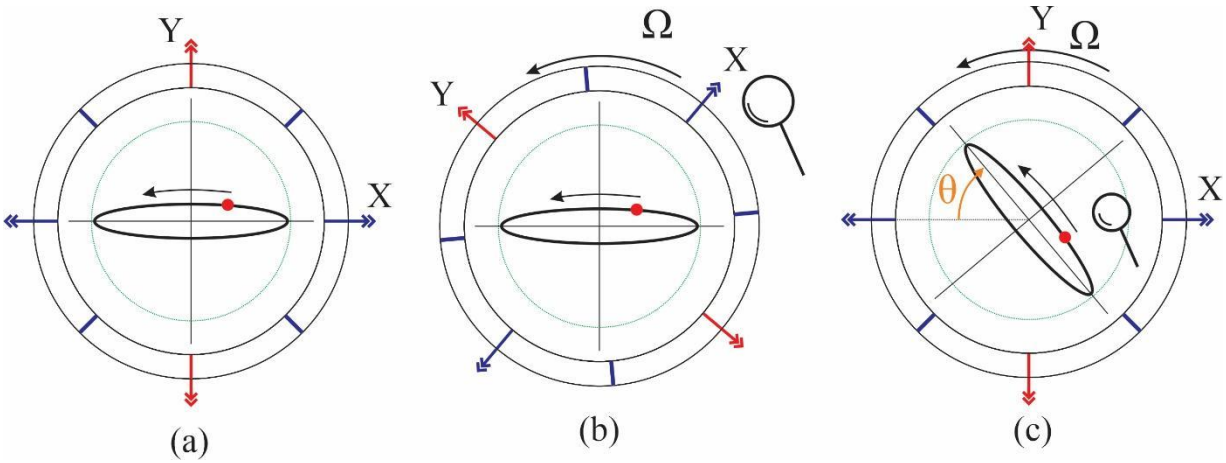

Figure 1. Evolution of the oscillation pattern in a RIG in the presence of rotation. As shown in (b), the oscillation pattern is stationary seen by an observer in an inertial coordinate frame. In the reference non-inertial coordinate frame attached to the sensing element, the oscillation pattern precesses, as shown in (c).

In reality, energy dissipation mechanisms cannot be neglected and asymmetries in the resonator cause anisoelasticity – a difference in the resonant frequencies. The EOM which captures these non-idealities is shown below:

$$\begin{bmatrix}\ddot{x}\\ \ddot{y}\end{bmatrix} + 2\kappa\Omega\begin{bmatrix}0 & -1\\ 1 & 0\end{bmatrix}\begin{bmatrix}\dot{x}\\ \dot{y}\end{bmatrix} + \begin{bmatrix}\omega_n^2 & 0\\ 0 & \omega_n^2\end{bmatrix}\begin{bmatrix}x\\ y\end{bmatrix} + \varepsilon_l = \begin{bmatrix}f_x\\ f_y\end{bmatrix}, \quad (3)$$

where ε_l denotes the non-idealities of a linear gyroscope resonator defined as

$$\varepsilon_l = 2\begin{bmatrix}\mu_x & \mu_{xy}\\ \mu_{xy} & \mu_y\end{bmatrix}\begin{bmatrix}\dot{x}\\ \dot{y}\end{bmatrix} + \begin{bmatrix}\beta_x & \beta_{xy}\\ \beta_{xy} & \beta_y\end{bmatrix}\begin{bmatrix}x\\ y\end{bmatrix} \quad (4)$$

μ_x, μ_y, and μ_{xy} represent the anisodamping coefficients and parameters β_x, β_y, and β_{xy} correspond to asymmetries in elasticity along the X and Y axes. The off-diagonal elements in the elasticity and damping matrices are used to capture a misalignment between the principal axes of elasticity and damping and the reference XY coordinates. In the presence of these non-idealities, the energy in the resonator dissipates with each oscillation and precession is negatively affected by the asymmetries in elasticity and damping, i.e., $\dot{\theta} \neq \kappa\Omega$ [2-5]. In a non-ideal RIG, the Whole Angle (WA) control architectures reported in [1],[3] can be employed to maintain the energy in the resonator and compensate for anisoelasticity through the control forces f_x and f_y shown on the right-hand side of Eq. (3).

As a result of anisoelasticity in the mechanical structure of an RIG, the oscillation trajectory, which is ideally a straight line, turns into an elliptical shape and the ellipticity affects the precession [5]. In practice, electrostatic frequency tuning can be employed to reduce anisoelasticity by matching the diagonal elements (i.e., $\beta_x = \beta_y$) and reducing the off-diagonal element β_{xy}. Additionally, a quadrature control architecture can be utilized to apply control forces for reducing ellipticity [1],[3]. It should be noted that a quadrature control architecture cannot fully eliminate quadrature (ellipticity). This is due to the inherent limitation of Proportional-Integral (PI) controllers in dealing with harmonic time-varying perturbations, which is studied in our recent publication [5].

In an ideal RIG, the estimation of the pattern angle using the vibration amplitude along the X and Y axes is similar to phase estimation in harmonic signals based on their in-phase and in quadrature components, which are recovered through a synchronous demodulation process. Similar to phase noise in electrical signals, the resolution in recovering the pattern angle is inversely proportional to the amplitude of the signal, [6], i.e., the amplitude of the

mechanical vibration denoted by a in Eq. (2). Therefore, to increase the Signal-to-Noise Ratio (SNR), it is necessary to operate the RIG with a larger amplitude of vibration, and at the extreme, in a non-linear regime. The EOM in Eq. (3) does not capture non-linear effects. To have a more accurate mathematical model, we need to include the non-linear mechanisms as well. The more commonly studied non-linear mechanisms in capacitive MEMS gyroscopes include the nonlinearity in electrostatic forces, the non-linear electro-mechanical restoration forces, and the nonlinearity in capacitive detection [7-11].

The non-linearity in the electrostatic control forces is out of the scope of this study. The nonlinearity in capacitive detection has been studied in [7] and a method for compensation is reported, which we reviewed and utilized in this work. As reported in [7,8], by operating a gyroscope in the non-linear regime, the elasticity in the reference XY coordinates becomes coupled to the amplitude of vibration. Hence, the concept of anisoelasticity as defined in linear 2DoF resonators does not hold.

This paper studies, analytically and experimentally, the effect of non-linear resonator dynamics on precession and the limitations of a quadrature controller in compensating the nonlinearity-induced-anisoelasticity. Also, to overcome the limitations, we investigate a modified WA control architecture for compensation of nonlinearity, so we can benefit from a high SNR at large vibration amplitude without introducing angle bias errors.

2. Amplitude-Dependent Anisoelasticity

As previously discussed, we need to account for nonlinearity in the restoration forces to have a more accurate mathematical model of a RIG. The geometrical and electrostatic nonlinearity in MEMS resonators affect the stiffness for deformations beyond the linear regime [11]. In the case of lumped-mass MEMS gyroscopes below 50 kHz, such as the Dual Foucault Pendulum (DFP), [12], the non-linear dynamics for a displacement below 15% of the capacitive gap size can be modeled as a Duffing nonlinearity. The Duffing nonlinearity in the DFP gyroscope has been reported to be dominantly an adverse effect of the electrostatic forces, which are intentionally used for mode-matching the gyroscope [9]. This assumption simplifies the derivations since the dynamics can be modeled through

$$\begin{bmatrix}\ddot{x}\\ \ddot{y}\end{bmatrix} + 2\kappa\Omega\begin{bmatrix}0 & -1\\ 1 & 0\end{bmatrix}\begin{bmatrix}\dot{x}\\ \dot{y}\end{bmatrix} + \begin{bmatrix}\omega_n^2 & 0\\ 0 & \omega_n^2\end{bmatrix}\begin{bmatrix}x\\ y\end{bmatrix} + \varepsilon_l + \varepsilon_{nl} = \begin{bmatrix}f_x\\ f_y\end{bmatrix}, \tag{5}$$

$$\varepsilon_{nl} = \begin{bmatrix}D_x & 0\\ 0 & D_x\end{bmatrix}\begin{bmatrix}x^3\\ y^3\end{bmatrix}, \tag{6}$$

where ε_{nl} represents the non-idealities that are associated with the non-linear resonator dynamics; parameters D_x and D_y denote the Duffing coefficients with expressions reported in [9]. The third-order nonlinearity terms independently cause a direct coupling between the elasticity along the X axis and the vibration amplitude along the same direction, and the elasticity along Y and the vibration amplitude along the Y axis.

To better illustrate the effect of nonlinearity on RIG operation and find the required control forces for compensation of nonlinearity, we use the following EOM

$$\begin{bmatrix}\ddot{x}\\ \ddot{y}\end{bmatrix} + 2\kappa\Omega.S\begin{bmatrix}\dot{x}\\ \dot{y}\end{bmatrix} + C\begin{bmatrix}\dot{x}\\ \dot{y}\end{bmatrix} + \lambda\begin{bmatrix}x\\ y\end{bmatrix} + D\begin{bmatrix}x^3\\ y^3\end{bmatrix} = \begin{bmatrix}f_x\\ f_y\end{bmatrix}, \tag{7}$$

$$S = \begin{bmatrix}0 & -1\\ 1 & 0\end{bmatrix},\ C = \begin{bmatrix}\mu_x & \mu_{xy}\\ \mu_{xy} & \mu_y\end{bmatrix},\ \lambda = \begin{bmatrix}\omega_x^2 & \omega_{xy}^2\\ \omega_{xy}^2 & \omega_y^2\end{bmatrix},\ D = \begin{bmatrix}D_x & 0\\ 0 & D_x\end{bmatrix} \tag{8}$$

EOM (7) and (5) are identical except that in Eq. (7), we used parameters ω_x^2, ω_y^2, and ω_{xy}^2 to represent the elasticity along the X and Y axes, and the coupling stiffness. As reported in [13], the method of averaging can be used to show that

$$D\begin{bmatrix}x^3\\ y^3\end{bmatrix} = \frac{3}{4}D\begin{bmatrix}|x|^2 & 0\\ 0 & |y|^2\end{bmatrix}\begin{bmatrix}x\\ y\end{bmatrix} \tag{9}$$

This derivation assumes that quadrature is orders of magnitude smaller than the vibration along the major axis of the elliptical pattern ($q \ll a$ in Fig. 2). As a result, the EOM in (7) can be rewritten as

$$\begin{bmatrix}\ddot{x}\\ \ddot{y}\end{bmatrix} + 2\kappa\Omega.S\begin{bmatrix}\dot{x}\\ \dot{y}\end{bmatrix} + C\begin{bmatrix}\dot{x}\\ \dot{y}\end{bmatrix} + \bar{\lambda}\begin{bmatrix}x\\ y\end{bmatrix} = \begin{bmatrix}f_x\\ f_y\end{bmatrix}, \tag{10}$$

$$\bar{\lambda} = \begin{bmatrix}\omega_x^2 + \frac{3}{4}D_x|x|^2 & \omega_{xy}^2\\ \omega_{xy}^2 & \omega_y^2 + \frac{3}{4}D_y|y|^2\end{bmatrix} \tag{11}$$

It is noted that for a symmetric structure with identical natural frequencies ($\omega_x = \omega_y,\ \omega_{xy} = 0$), the resonant frequencies along the X and Y directions will not be identical as the amplitude of vibration increases and the difference would depend on the vibration amplitude along the X and Y directions and the Duffing coefficients.

Furthermore, the amplitude-frequency coupling caused by electrostatic nonlinearity follows a quadratic function of the amplitude of vibration, as shown in Eq. (11), and to reach the

ideal RIG described in Eq. (1), we would need to compensate for linear imperfections (anisodamping and anisoelasticity represented by ε_l) and the non-linear imperfections (ε_{nl}).

To investigate the effect of nonlinearity on precession in RIG, we rewrote the EOM in a coordinate frame along and perpendicular to the line of oscillation at a given instance t_i. To go from the reference XY coordinate frame to the $X'Y'$ frame, we use the following transformation

$$\begin{bmatrix} x' \\ y' \end{bmatrix} = R(-\theta) \begin{bmatrix} x \\ y \end{bmatrix} \quad , \quad R(-\theta) = \begin{bmatrix} cos\,\theta & sin\,\theta \\ -sin\,\theta & cos\,\theta \end{bmatrix}, \tag{12}$$

where θ is the pattern angle shown in Fig. 2.

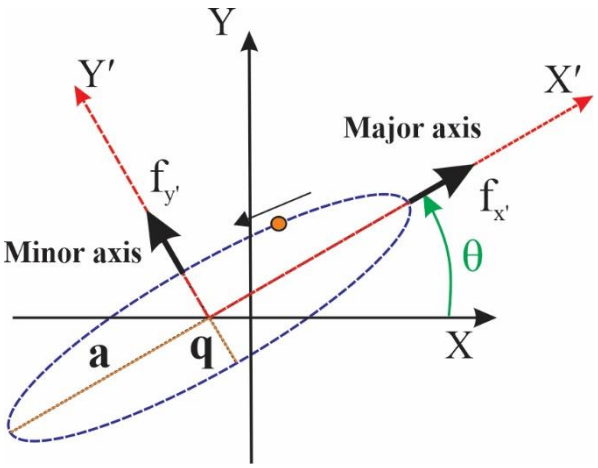

Figure 2. Elliptical pattern of oscillation in a RIG. The reference coordinate frame (XY) and the coordinate along the line of oscillation ($X'Y'$) is illustrated.

Assuming that the angular velocity of rotation (Ω) is orders of magnitude smaller than the angular velocity of oscillation (ω), the EOM in $X'Y'$ coordinate frame takes the following form

$$\begin{bmatrix} \ddot{x}' \\ \ddot{y}' \end{bmatrix} + 2\kappa\Omega.S' \begin{bmatrix} \dot{x}' \\ \dot{y}' \end{bmatrix} + C' \begin{bmatrix} \dot{x}' \\ \dot{y}' \end{bmatrix} + \lambda' \begin{bmatrix} x' \\ y' \end{bmatrix} = \begin{bmatrix} f_{x'} \\ f_{y'} \end{bmatrix}, \tag{13}$$

To reach a near-ideal operation, described by Eq. (1), the ellipticity of oscillation must be eliminated and the amplitude of vibration along the major axis must be maintained. With that goal in mind, the following control forces must be applied at instance t_i along the X' and Y' directions

$$\begin{cases} f_{x'}(t_i) = C'_{11}(t_i)\,\dot{x}'(t_i) \\ f_{y'}(t_i) = \lambda'_{21}(t_i)\,x'(t_i) \end{cases}, \tag{14}$$

as a result, the differential equation (13) reduces to

$$\begin{cases} \ddot{x'} + \lambda'_{11}x' = 0 \\ \ddot{y'} + \mathrm{C}'_{22}\dot{y'} + (2\kappa\Omega S'_{21} + C'_{21})\dot{x'} + \lambda'_{22}y' = 0 \end{cases} \quad (15)$$

It should be noted that at instance t_i, the vibration along the Y' axis is zero, based on our definition of the $X'Y'$ coordinate frame. In equation (15), the parameter $S'_{21} = 1$ and with an assumption that $x' = a\,cos\,(\varphi)$, expressions for λ'_{11}, C'_{11}, and λ'_{21} can be derived from Eq. (10) and (12) as

$$\lambda'_{11} = \tfrac{1}{2}\left(\omega_x^2 + \omega_y^2\right) + \tfrac{1}{2}\cos 2\theta\left(\omega_x^2 - \omega_y^2\right) + \sin 2\theta\,\omega_{xy}^2 + \tfrac{3}{4}\mathrm{a}^2(D_x\cos^4\theta + D_y\sin^4\theta) \quad (16)$$

$$C'_{11} = \tfrac{1}{2}\left(\mu_x + \mu_y\right) + \tfrac{1}{2}cos\,2\theta\left(\mu_x - \mu_y\right) + sin\,2\theta\,\mu_{xy} \quad (17)$$

$$\lambda'_{21} = \tfrac{1}{2}sin\,2\theta\left(\omega_y^2 - \omega_x^2\right) + cos\,2\theta\,\omega_{xy}^2 + \tfrac{3}{8}sin\,2\theta\,\mathrm{a}^2(D_x\cos^2\theta - D_y\sin^2\theta) \quad (18)$$

These equations indicate that by applying control forces defined in (15), (17), and (18) the vibration along X' would be maintained and the vibration along Y' is eliminated. The angular velocity of oscillation along X' will be equal to $\dot{\varphi} = \sqrt{\lambda'_{11}}$ at t_i, where λ'_{11} is defined in Eq. (16).

By assuming that the amplitude of vibration is in the linear range ($D_x a^2 \approx D_y a^2 \approx 0$), the equations (16)-(18) reduce to

$$\lambda'_{11} = \tfrac{1}{2}\left(\omega_x^2 + \omega_y^2\right) + \tfrac{1}{2}cos\,2\theta\left(\omega_x^2 - \omega_y^2\right) + sin\,2\theta\,\omega_{xy}^2 \quad (19)$$

$$\beta'_{11} = \tfrac{1}{2}\left(\mu_x + \mu_y\right) + \tfrac{1}{2}cos\,2\theta\left(\mu_x - \mu_y\right) + sin\,2\theta\,\mu_{xy} \quad (20)$$

$$\lambda'_{21} = \tfrac{1}{2}sin\,2\theta\left(\omega_y^2 - \omega_x^2\right) + cos\,2\theta\,\omega_{xy}^2 \quad (21)$$

By using the commonly used quantities $\omega, \Delta\omega, \frac{1}{\tau}$, and $\Delta\left(\frac{1}{\tau}\right)$, which are defined in [3] as the average resonant frequency, frequency split, average reciprocal of energy decay time constants, and the different in reciprocal of energy decay time constants, equations (19)-(21) become identical to the solution of the differential equations derived for evolution of the orbital oscillation in RIG reported in the same article.

The results in (16) indicate that in a RIG with an amplitude of vibration in the linear range, the elasticity changes harmonically with a 2θ dependency with a magnitude proportional to

$\Delta\omega$. For amplitudes of vibration in the non-linear range, the resonant frequency changes with a larger magnitude and a 4θ dependency due to the non-linear dynamics. The same conclusions apply to the quadrature control force $f_{y'}$ in Eq. (14).

In the operation of RIG, independent of the vibration amplitude, the WA control proposed in [3] utilizes the 'Q' pendulum variable and calculates the quadrature control force (f_q) to suppress ellipticity. Due to the inherent limitation of the PI feedback in the quadrature control architecture in tracking a harmonic time-varying perturbation, the output would be an underestimate or overestimate of the ideal quadrature control force f_y' in Eq. (14) and (21). As a result, we hypothesized that as the vibration amplitude is increased, to benefit from an improved SNR, the residual quadrature during precession would increase nonlinearly with the amplitude of vibration. In turn, angle-dependent biases and angular drift due to the reduction of the effective angular gain are introduced.

3. Validation of the Model

In this section, we present experimental result on instrumenting a MEMS Dual Foucault Pendulum (DFP) gyroscope [12], as a RIG to test our hypothesis. The DFP used in our experiments is shown In Fig. 3.

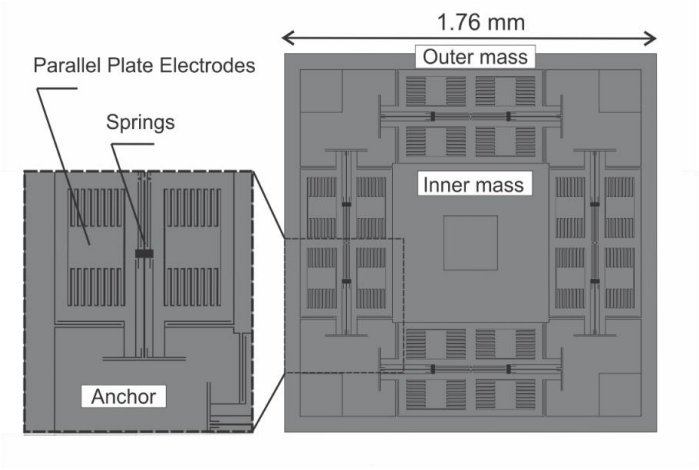

Figure 3. Design of the DFP gyroscope, which was used for experimental validation of the analytical results. As annotated, in the DFP gyroscope design parallel plate electrodes were used for motion actuation, detection, and electrostatic frequency tuning.

The axisymmetric DFP gyroscope design architecture consisted of inner and outer masses that moved in an anti-phase motion along the X and Y axes. The DFP device with a footprint less than 4 mm^2 was fabricated with a 40 µm-thick device layer. The nominal operational frequency and quality factor of the DFP were measured on the order of 15 kHz and 1.1 M,

respectively. Details on design parameters and fabrication process of the DFP gyroscope can be found in [13].

As the first experiment, the closed-loop WA control, as described in [3], was implemented with a Zurich HF2Li lock-in amplifier using the Real-Time Kit (RTK) module, [16]. Using the method reported in [15], gain-mismatches in the detection and control electronics along the X and Y axes were identified and compensated. The device was characterized on an Ideal Aerosmith 1291BR rate-table, and the local temperature-variation around the Leadless Chip Carrier (LCC)-packaged DFP was controlled to within 10mK. We applied a 360 Degree-Per-Second (DPS) physical rotation to the DFP using the rate table and measured the orientation of the oscillation pattern. The precession using the MEMS DFP RIG is shown in Fig. 4.

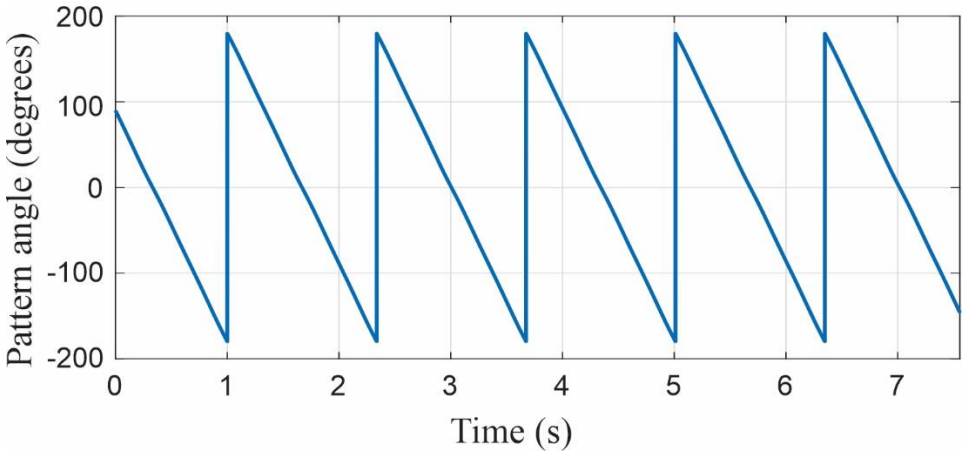

Figure 4. Precession in the DFP RIG. The pattern angle is shown for a 360 DPS rotation input, which measures an angular gain (κ) on the order of 0.76.

As previously explained, the WA control proposed in [3] utilizes the $'Q'$ pendulum variable and calculates the quadrature control force; the reference phase is set to the phase of oscillation tracked using a Phase-Locked Loop (PLL). In the case of applying the WA control to the DFP gyroscope, variations of quadrature control force and the actuation frequency (tracked frequency of oscillation) for different vibration amplitudes are shown in Fig.5.

As illustrated in Fig. 5(a), the variation of the oscillation frequency through precession is very small at an amplitude of vibration equal to 1.5% of the capacitive gap size. This is due to the fact that as an initial step of the experiment, we identified appropriate DC voltages for electrostatic tuning of the DFP gyroscope to minimize the difference in the diagonal terms of the stiffness matrix ($\omega_x \approx \omega_y$). In this step, the frequency split of the DFP was reduced from 114 Hz to 30 mHz by applying 8.3 V and 3.009 V biasing voltages to the X and Y parallel electrodes, respectively.

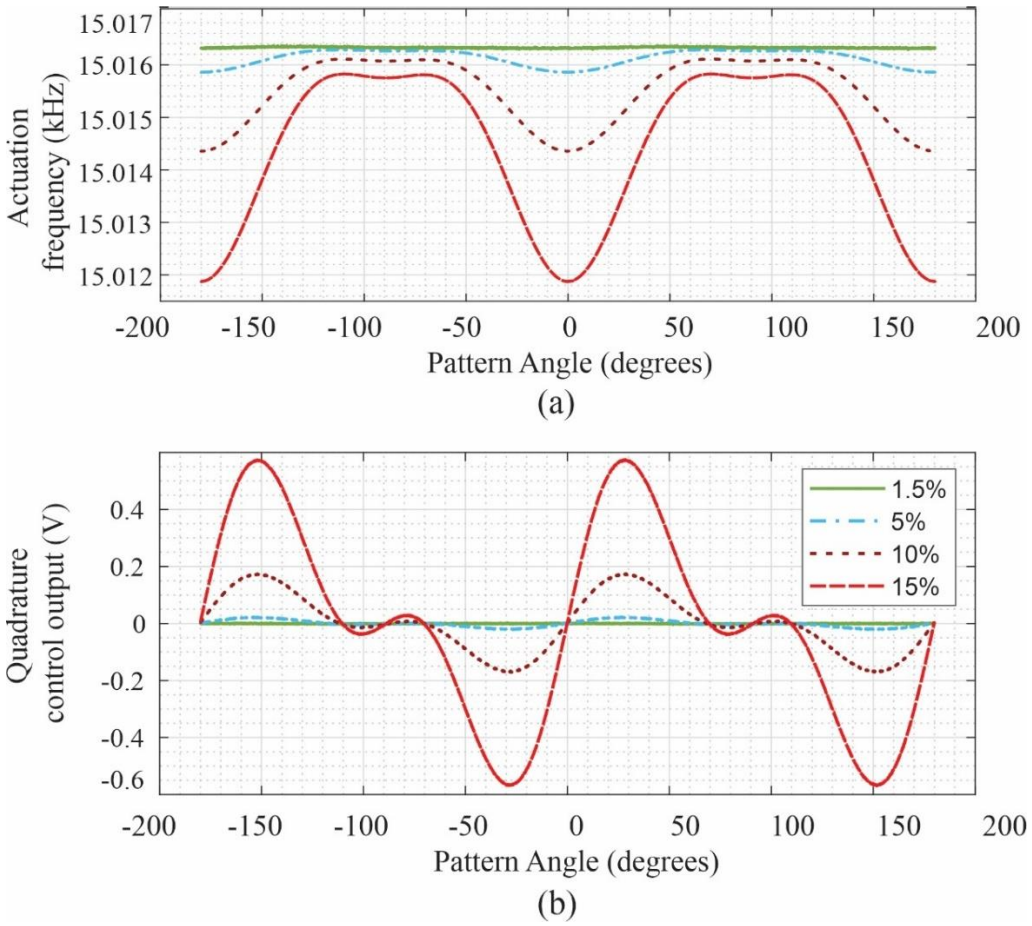

Figure 5. Experimental data on variations of the tracked frequency (a) and quadrature control voltage(b), for different vibration amplitudes. It is demonstrated that due to non-linear dynamics, isoelasticity in gyroscope is negatively affected at a larger vibration amplitude. As shown, due to the induced anisoelasticity higher control voltages were required to suppress quadrature.

As observed in Fig. 5(a), at higher amplitude of vibration the electrostatic nonlinearity resulted in higher variations in the oscillation frequency during precession. This agrees with Eq. (16) confirming that the amplitude-frequency coupling along the X and Y axes cause angle dependent and amplitude dependent variations in the elasticity during precession. Similarly, since anisoelasticity increased with the amplitude of vibration, the quadrature control voltage which was required to suppress ellipticity increased nonlinearly shown in Fig. 5(b). This result agrees with the expression in Eq. (18).

During precession, since we are dealing with time-varying perturbations, a PI feedback loop overestimates or underestimates the control forces and the phase of oscillation [9]. Therefore, residual quadrature and phase errors are inevitable. To demonstrate this, the measured quadrature to energy ratio is shown in Fig. 6 for different amplitude of vibration. This result confirmed our hypothesis that due to a higher anisoelasticity induced by nonlinearity the residual quadrature increases at larger vibration amplitude. It is also shown

that at higher amplitude of vibration due to the higher residual quadrature the angular gain was reduced, in agreement with the results in [5].

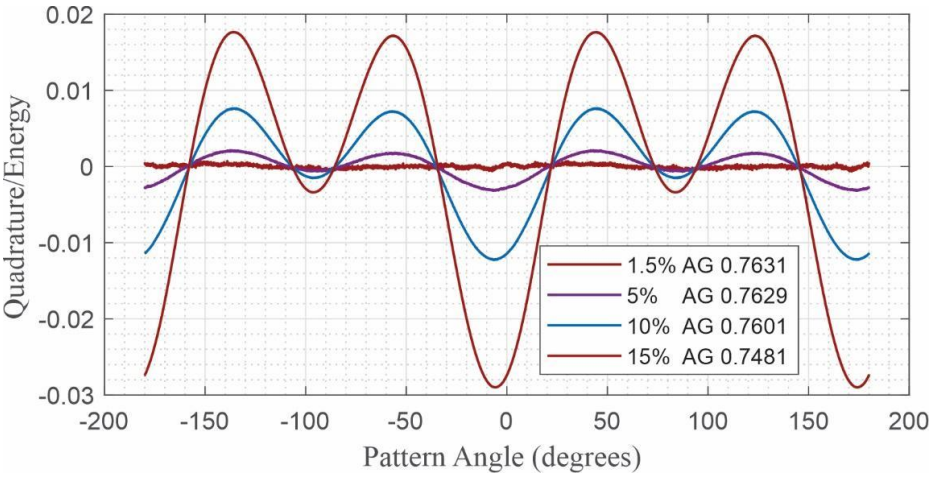

Figure 6. Experimentally characterized residual quadrature-to-energy ratio for different vibration amplitudes. Due to anisoelasticity caused by nonlinearity, at a higher amplitude of vibration, quadrature and angular gain were observed to increase and reduce, respectively.

4. A Modified WA Control

The experimental results confirmed that operation in the non-linear regime would increase the ellipticity and introduce angular drift in RIG. In this section, we propose a modification to the WA control based on Eq. (7)-(9) for compensation of the Duffing nonlinearity.

To eliminate amplitude-frequency coupling along the X and Y axes, we are required to apply independent feedback forces along the X and Y directions with a magnitude proportional to the cube of the amplitude of vibration in that direction, i.e., $|x|^3, |y|^3$ for X and Y direction, respectively, and in-phase to the oscillation phase. As shown in Fig. 7, the modified control requires the nonlinearity coefficients (D_x and D_y), the amplitude of vibration (a), the electrostatic actuation gains, and the instantaneous pattern angle (θ). As the core of this control architecture, we still rely on the conventional WA control, reported in [3], to calculate the pattern angle, the pendulum variables, and compensate for energy dissipation and residual anisoelasticity.

This modification would effectively eliminate the amplitude-frequency coupling and reduce the amplitude and angle dependency of anisoelasticity. In practice, the Duffing coefficients can be characterized empirically based on Eq. (16) through a ring down approach similar to the method proposed in [11]. However, as mentioned before, for the feedback control architecture a knowledge of the actuation gains is also essential.

An alternative method to identify these parameters is to apply the nonlinearity compensation forces during operation and to incrementally change values of D_x and D_y, and measure the actuation frequency at different amplitudes of vibration. The optimized parameters would yield the lowest variation of resonant frequency as a function of the vibration amplitude, i.e., the lowest amplitude-frequency coupling. It should be noted that the parameters D_x and D_y can be optimized independently in a RIG by locking the pattern angle to zero and ninety degrees, respectively, using a rate control loop [3]. In this study, the second approach was followed to identify the Duffing nonlinearity coefficients.

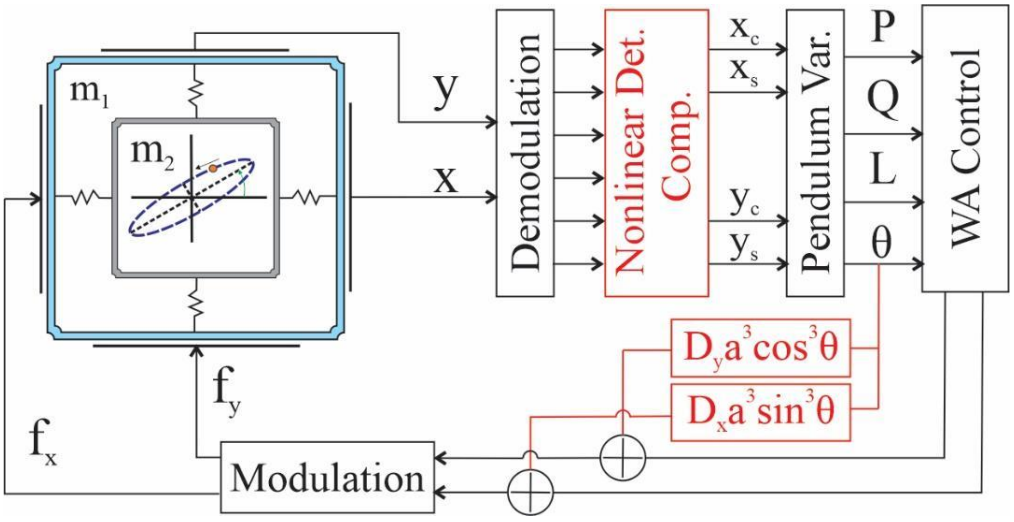

Figure 7. The modified WA control architecture for RIG operation in the non-linear regime. Based on the method reported in [7], the demodulated signals were modified to eliminate non-linearity in capacitive detection. Additional control forces (shown in red) were applied along with the conventional WA control forces to compensate for Duffing nonlinearity.

Additionally, since the DFP uses parallel plate electrodes for capacitive motion detection, our measurements of displacement would be highly non-linear. The nonlinearity in capacitive detection results in a higher conversion gain, from displacement to current, as the vibration amplitude increases [17]. In rate-integrating gyroscopes, since we rely on the amplitude of vibration along the X and Y axes to estimate the pattern angle, the nonlinearity would negatively affect our estimations and result in angle errors. As part of the modified WA control, we utilized the method reported in [7] to minimize the nonlinearity in capacitive detection. As part of this method, we used an amplitude dependent correction gain to compensate for the non-linear capacitive detection gain.

Assuming that our demodulation signals along the X and Y axes are x_s, x_c, y_s, and y_c, we used the modified measurements as shown below for estimation of the pendulum variables

$$\begin{cases} x'_c = x_c(1-\delta(x_s^2+x_c^2)) \\ x'_s = x_s(1-\delta(x_s^2+x_c^2)) \\ y'_c = y_c(1-\delta(y_s^2+y_c^2)) \\ y'_s = y_s(1-\delta(y_s^2+y_c^2)) \end{cases} \quad (22)$$

where parameter δ is a function of the capacitance, gap size, carrier voltage, and the transimpedance gain. In our experiments, δ was identified empirically through a method similar to what is reported in [15] for identification of capacitive detection gain mismatch in RIG.

The detection nonlinearity results in an angle-dependent bias (ADB), which is only correlated to δ and the amplitude of vibration (a). The ADB due to capacitive nonlinearity can be decoupled from other error sources by rotating the RIG at high angular rate (in this study, we used 500 DPS rotation). The ADB measured at 500 DPS can be used to directly extract or fine tune δ to minimize ADB. In the case of the DFP, δ was characterized to be on the order of 1.006.

By implementing the modified WA control with the DFP gyroscope, we were able to significantly reduce the nonlinearity-induced-anisoelasticity at larger amplitudes of vibration, shown in Fig. 8, and minimize the nonlinearity in capacitive detection. As shown in Fig. 8(a), the nonlinearity compensation forces reduced variations of the oscillation frequency during precession from 4Hz to 50 mHz. As a result, the quadrature to energy ratio (Fig. 8(b)) was reduced by more than 100x, down to 300ppm, which in turn, increased the angular gain of the DFP to its effective value measured for the linear operation condition on the order of 0.7631, shown in Fig. 6.

To demonstrate the improvement in noise performance and reduction of angle-dependent bias, we measured the angle error of the DFP RIG ($\theta_{error} = \theta_{output} - \int \Omega \, dt$) and applied a Fast Fourier Transform (FFT), shown in Fig. 9. By employing a high amplitude of vibration equal to 15% of the capacitive gap size and compensating for the Duffing nonlinearity and capacitive nonlinearity, we were able to achieve an angle white noise on the order of 0.4 mdegree/√Hz and angle random walk of 4.2 mdegree/√s.

5. Discussion and Conclusion

In this paper, we presented analytical and experimental results to explain the trade-off between achieving a higher SNR in RIG through increasing the amplitude of vibration and the adverse non-linear effects on operation. We introduced a modified WA control architecture which significantly reduced anisoelasticity at large amplitude of vibration to benefit from the high SNR while maintaining a low angular error.

Based on the experimental results, one limitation in our approach was the impractically large AC voltages which were required as part of the control system for compensation of nonlinearity and quadrature at high amplitude of vibration, Fig.5(b). As a reference, an AC signal less than 5 mV was required to achieve an amplitude of vibration equal to 15% of the capacitive gap size for the DFP gyroscope with a quality factor around 1.1M. On the other hand, AC voltages on the order of 1-2 V were required to compensate for nonlinearity. From Eq. (14), (18), it is evident that increasing the amplitude of vibration beyond 15% would require control voltages in the tens of volts range.

Interestingly, we observed that the high AC control voltages, coupled with the nonlinearity of electrostatic forces, modulated a variation on the resonant frequency, which could not be eliminated through our nonlinearity compensation method, which can be observed in Fig. 8.

The second and more important challenge in having a high ratio between the control voltage required for suppressing quadrature/nonlinearity and the voltage to maintain the energy was the adverse effects on stability of RIG operation. Since phase drifts in control electronics are inevitable, cross-coupling between the quadrature control loop and the rate control loop is also inevitable [3],[15]. Therefore, using excessively large control voltages for quadrature compensation coupled with phase drifts in electronics would negatively affect the angular gain stability and result in drift in angle measurements.

Therefore, we believe that while in theory control architectures such as the one developed in this study can be designed to compensate for non-idealities in RIG, they should be used advertently. Our results highlight the need for fabrication of structurally symmetric micro-gyroscopes which would not rely on high biasing voltage for tuning; as demonstrated in this paper, the biasing voltages would result in nonlinearity and affect RIG operation at higher amplitudes of vibration limiting the resolution and accuracy of angle measurements.

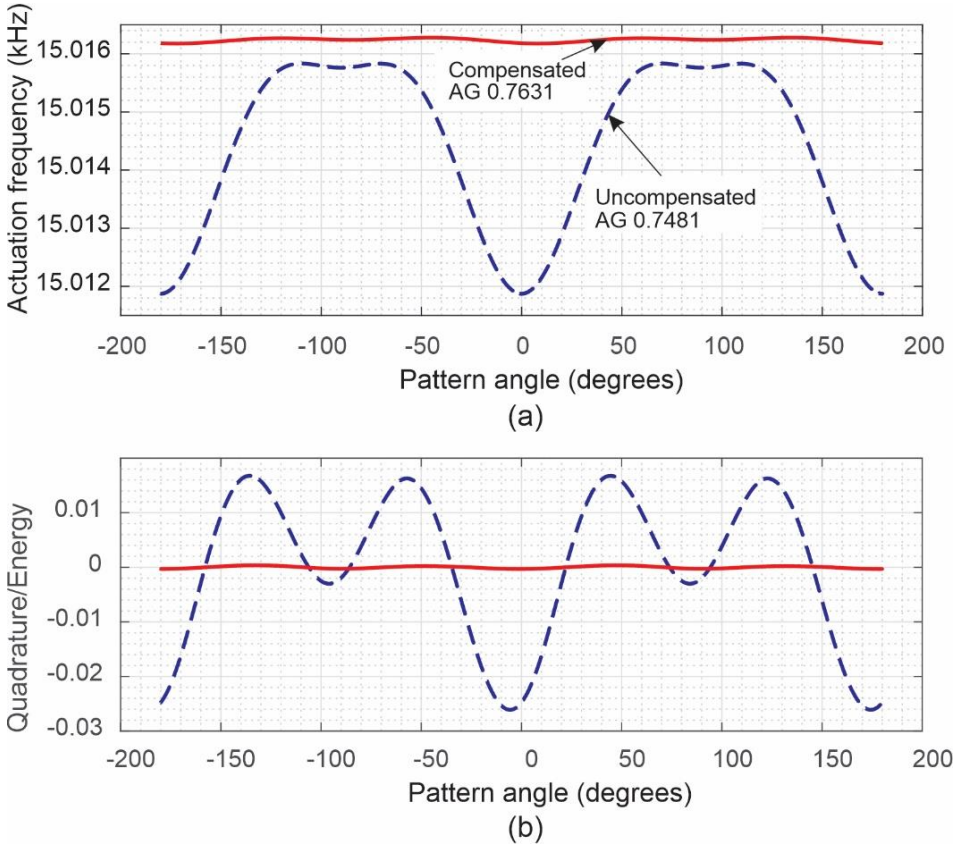

Figure 8. Variations of elasticity (a) and residual quadrature (b), at a vibration amplitude equal to 15% of the capacitive gap size, were reduced through compensation of the Duffing non-linearity.

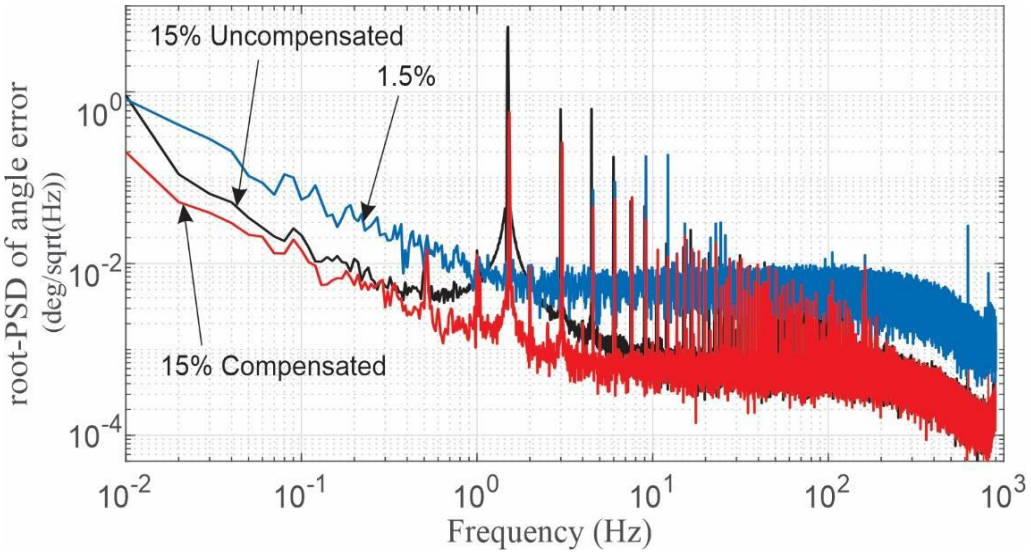

Figure 9. Comparison of the root-PSD of angle error in a DFP RIG. It is demonstrated that by increasing the vibration amplitude, the Angle White Noise (AWN) and Angle Random Walk (ARW) were improved; however, angle bias errors were introduced. Through compensation of Duffing non-linearity and the residual quadrature, the angle biases were reduced by a factor of 10.

References

[1] M. F. Hutton and B. Friedland. Control system for angular displacement sensor, November 23 1976. US Patent 3,992,952.

[2] B. Friedland and M. Hutton. Theory and error analysis of vibrating-member gyroscope. IEEE Transactions on Automatic Control, vol. 23, no. 4, pp. 545–556, August 1978.

[3] D. D. Lynch. Vibratory gyro analysis by the method of averaging. In Proceedings of St. Petersburg Conference on Gyroscopic Technology and Navigation, St. Petersburg, May 1995.

[4] I. P. Prikhodko, J. A. Gregory, D. I. Bugrov, and M. W. Judy. Overcoming limitations of rate integrating gyroscopes by virtual rotation. In IEEE International Symposium on Inertial Sensors and Systems (INERTIAL), Laguna Beach, CA, USA, February 2016.

[5] D. Vatanparvar and A. M. Shkel. On correlation of anisoelasticity, angular gain, and temperature in whole-angle CVGs. In IEEE Sensors Journal, vol. 22, no. 5, pp. 4175-4185, March 2022.

[6] P.Ward and A. Duwel. Oscillator phase noise: Systematic construction of an analytical model encompassing nonlinearity. IEEE Transactions on Ultrasonics, Ferroelectrics, and Frequency Control, vol. 58, no. 1, pp. 195–205, January 2011.

[7] Z. Hu and B. J. Gallacher. Effects of nonlinearity on the angular drift error of an electrostatic MEMS rate integrating gyroscope. IEEE Sensors Journal, vol. 19, no. 22, pp. 10271-10280, November 2019.

[8] S. H. Nitzan, P. Taheri-Tehrani, M. Defoort, S. Sonmezoglu, and D. A. Horsley. Countering the effects of nonlinearity in rate-integrating gyroscopes. IEEE Sensors Journal, vol. 16, no. 10, pp. 3556–3563, February 2016.

[9] D. Vatanparvar and A. M. Shkel. Instabilities due to electrostatic tuning of frequency split in coriolis vibratory gyroscopes. In IEEE Sensors Conference (SENSORS), Rotterdam, Netherlands, October 2020.

[10] D. Vatanparvar and A. Shkel. Effect of electrostatic nonlinearity on force-to-rebalance mode of operation in CVG. In DGON Inertial Sensors and Systems (ISS), Braunschweig, Germany, September 2020.

[11] P. M. Polunin, Y. Yang, M. I. Dykman, T. W. Kenny, and S. W. Shaw. Characterization of MEMS Resonator Nonlinearities Using the Ringdown Response. Journal of Microelectromechanical Systems, vol. 25, no. 2, pp. 297-303, April 2016.

[12] D. Senkal, S. A. Zotov, and A. M. Shkel. Fully balanced micro-machined inertial sensor, April 2 2019. US Patent 10,247,554.

[13] M. H. Asadian, S. Askari, I. B. Flader, Y. Chen, D. D. Gerrard, D. D. Shin, H.-K. Kwon, T. W. Kenny, and A. M. Shkel. High quality factor mode ordered dual Foucault pendulum gyroscope. In IEEE Sensors Conference (SENSORS), New Delhi, India, October 2018.

[14] N. N. Bogoliubov. Asymptotic methods in the theory of non-linear oscillations, volume 10. CRC Press, 1961.

[15] D. Vatanparvar and A. M. Shkel. Identification of gain mismatches in control electronics of rate integrating CVGs. In IEEE International Symposium on Inertial Sensors and Systems (INERTIAL), Kailua-Kona, HI, USA, March 2021.

[16] S. Askari, M. H. Asadian, and A. M. Shkel. High quality factor MEMS gyroscope with whole angle mode of operation. In IEEE International Symposium on Inertial Sensors and Systems (INERTIAL), Lake Como, Italy, March 2018.

[17] A. A. Trusov and A. M. Shkel. A Novel Capacitive Detection Scheme with Inherent Self-Calibration. Journal of Microelectromechanical Systems, vol. 16, no. 6, pp. 1324-1333, December 2007.